Phenomics (2022) 2:219–229
https://doi.org/10.1007/s43657-022-00063-0

ARTICLE

Palmprint Phenotype Feature Extraction and Classification Based on Deep Learning

Yu Fan[1] · Jinxi Li[2,3] · Shaoying Song[4] · Haiguo Zhang[5,6] · Sijia Wang[3,7] · Guangtao Zhai[1]

Received: 12 October 2021 / Revised: 8 May 2022 / Accepted: 12 May 2022 / Published online: 22 June 2022

Abstract

Palmprints are of long practical and cultural interest. Palmprint principal lines, also called primary palmar lines, are one of the most dominant palmprint features and do not change over the lifespan. The existing methods utilize filters and edge detection operators to get the principal lines from the palm region of interest (ROI), but can not distinguish the principal lines from fine wrinkles. This paper proposes a novel deep-learning architecture to extract palmprint principal lines, which could greatly reduce the influence of fine wrinkles, and classify palmprint phenotypes further from 2D palmprint images. This architecture includes three modules, ROI extraction module (REM) using pre-trained hand key point location model, principal line extraction module (PLEM) using deep edge detection model, and phenotype classifier (PC) based on ResNet34 network. Compared with the current ROI extraction method, our extraction is competitive with a success rate of 95.2%. For principal line extraction, the similarity score between our extracted lines and ground truth palmprint lines achieves 0.813. And the proposed architecture achieves a phenotype classification accuracy of 95.7% based on our self-built palmprint dataset CAS_Palm.

Keywords Palmprint principal line extraction · Palmprint phenotype classification · ROI extraction · Deep learning

Introduction

Dermatoglyphics refers to the texture patterns of skin on certain body parts such as fingers, palms, and soles. During the early period of embryonic development, dermatoglyphics will develop into a certain pattern influenced by genotype and environment. Palmar creases were distinguished into major and minor creases. Major palmar creases, which are called "palmprint principal lines" in this study, consist of radial longitudinal crease, proximal transverse crease, and distal transverse crease, and have been analyzed qualitatively and quantitatively. Compared with other dermatoglyphics, palmprint has many advantages: palmprint feature can be obtained from low-resolution images while fingerprint

Yu Fan and Jinxi Li contributed equally.

✉ Sijia Wang
wangsijia@picb.ac.cn

✉ Guangtao Zhai
zhaiguangtao@sjtu.edu.cn

1 School of Electronic Information and Electrical Engineering, Shanghai Jiao Tong University, Shanghai 200240, People's Republic of China

2 State Key Laboratory of Genetic Engineering, Human Phenome Institute, Zhangjiang Fudan International Innovation Center, Fudan University, Shanghai 201203, People's Republic of China

3 CAS Key Laboratory of Computational Biology, Shanghai Institute of Nutrition and Health, University of Chinese Academy of Sciences, Chinese Academy of Sciences, Shanghai 200031, People's Republic of China

4 BGI College and Henan Institute of Medical and Pharmaceutical Sciences, Zhengzhou University, Zhengzhou 450052, People's Republic of China

5 Ministry of Education Key Laboratory of Contemporary Anthropology, Department of Anthropology and Human Genetics, School of Life Sciences, Fudan University, Shanghai 200438, People's Republic of China

6 School of Basic Medicine, Shanghai Jiao Tong University School of Medicine, Shanghai Jiao Tong University, Shanghai 200025, People's Republic of China

7 Center for Excellence in Animal Evolution and Genetics, Chinese Academy of Sciences, Kunming 650223, People's Republic of China

cannot; palmprint collection device is cheaper than iris collection device (Zhang et al. 2017).

Palmprint principal lines are the most dominant and are easy to get lines even in some low-resolution images, while other fine wrinkles and shorter lines may be missing. Palmprint principal lines contain rich information, which can be applied in palmprint recognition (Shu and Zhang 1998; Huang et al. 2008), personality prediction (Prasad and Chai 2020), medical conditions prediction (Cascos 1965; Wojtowicz and Wajs 2012) and many other fields. Based on the different distribution of three palmprint principal lines, we can divide palmprint phenotype into major four types: normal type, Sydney crease type, Simian crease type and Triple radial base crease, and Fig. 1 offers some examples of dermatoglyphics and palmprint.

This paper mainly pays attention to the extraction of palmprint principal lines and the classification of palmprint phenotype using these extracted principal lines, which provide ease for other large-scale population study rather than individual recognition. Palmprint principal line extraction and classification contain three steps: (a) ROI extraction, (b) palmprint principal line extraction and (c) palmprint phenotype classification. Traditional method usually utilizes manually designed filters in these three steps, which needs large labor effort and lacks robustness (Badrinath and Gupta 2012; Ali et al. 2016; Bruno et al. 2014). And the quality of palmprint images can have a high impact on the classification accuracy (Zhai and Min 2020; Zhai et al. 2005). To improve the performance of palmprint phenotype classification, we design deep learning modules for palmprint ROI extraction, principal line extraction, and classification. Each step has been optimized, and our contributions can be summarized as follows:

1. We introduce the first palmprint principal line extraction method using a deep edge detection model, and our results show our line extraction is more accurate than the traditional palmprint edge detection operator.
2. We propose a new deep learning palmprint phenotype classification architecture, including REM, PLEM, and

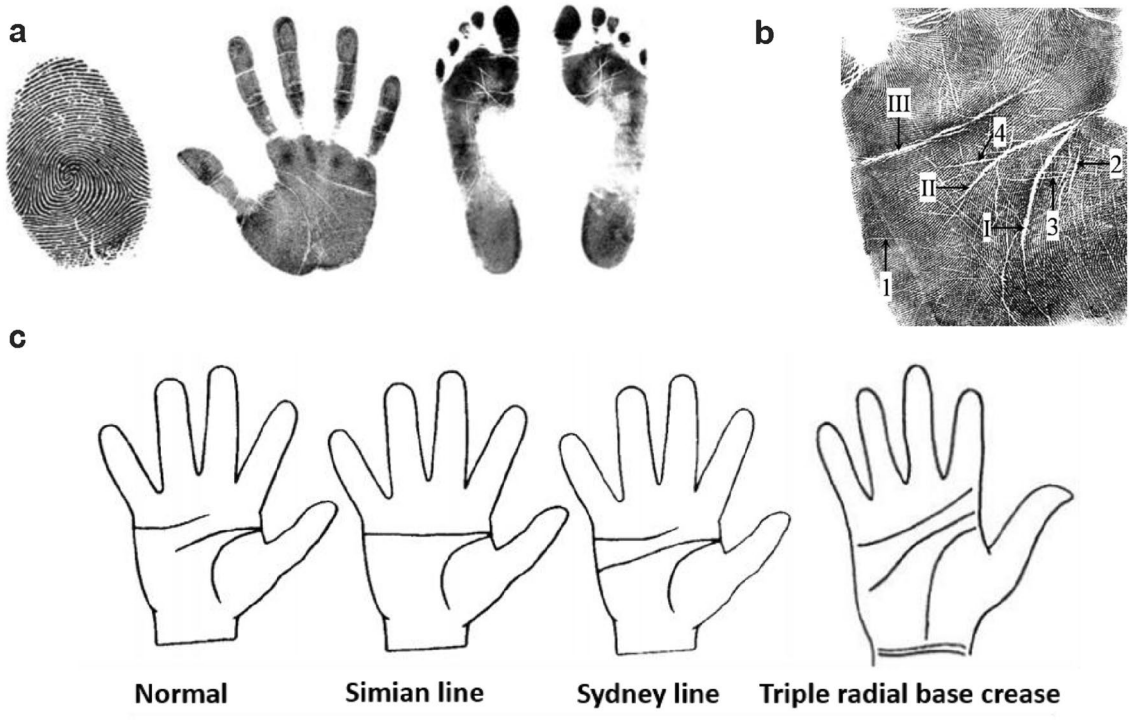

Fig. 1 Introduction of dermatoglyphics and palmprint **a** Three different kinds of human dermatoglyphics, from left to right is fingerprint, palmprint, and footprint. **b** Definition of palmar creases. Radial longitudinal crease (I) becomes distinct according to the flexion of carpometacarpal joints of the thumb. Proximal (II) and distal transverse creases (III) become distinct according to the flexion of the metacarpophalangeal joints of the second to fifth fingers. Other minor creases are not studied so far. **c** Four different palmprint phenotype class types, based on the different distribution of principal lines. Normal crease. Simian crease: proximal and distal transverse crease meet to cross the palm and so named as it resembles the usual condition of non-human simians (primates). Sydney crease: extended proximal palmar crease across the palm and so named as first described in Sydney, Australia. Triple radial base crease: radial longitudinal crease and proximal transverse crease do not meet on the radial border of the palm are also named Open crease (Park et al. 2010). Recently a new Suwon crease has been described as an extended distal transverse crease and so named as it first described in Suwon, Korea. In our study, we categorized the Suwon crease as Simian crease because of its rarity, which is lower than 0.5%

PC. Compared with the traditional method, our model has competitive results.
3. Since there is no proper dataset with palmprint phenotype, we introduce a new palmprint dataset, named CAS_Palm with manually labeled palmprint phenotype and palmprint principal lines.

The rest of the paper is organized as follows: we describe the architecture of our proposed method, and give the details of our experiments and results, then we discuss the results and conclude this paper.

Materials and Methods

Dataset

The database we used is a self-built palmprint database, including 5251 images collected from 5251 subjects, namely CAS_Palm. Both hands of each subject were scanned to a 6840 * 4824 image by using an EPSONV370 scanner. Different from the previous public palm dataset, such as the Hong Kong Polytechnic University Palm Dataset, our self-built CAS_Palm dataset has no requirements on the lighting environment where the subject is and the palm position, which requires the algorithm to be highly robust.

Proposed Architecture

The architecture of our proposed model is shown in Fig. 2, including three different modules: REM, PLEM and PC. REM will extract the ROI area from the palm images using a pre-trained hand key point location model. The output of REM, i.e. the ROI area, is the input of PLEM. PLEM will employ a deep edge detection model to extract three principal lines from ROI area, and PC will use a ResNet34 classifier to classify these palmprint images into different types based on their ROI area and principal lines. We will express the details of our model in the following section.

REM

The traditional ROI extraction method is based on valley point extraction. It first segments the palm from the background by setting a proper threshold, which is usually calculated adaptively (Otsu 1979). Then Kekre's method (Kekre et al. 2012) needs an edge detection algorithm to find the contour of the hand. The valley points are usually the points closest to the palm centroid in the contour. So the valley points are found and ROI can be extracted using the location of valley points.

But two problems may occur in the process: first, when the luminance condition is complex, it is difficult to find a proper threshold for palm segmentation. Second, when the fingers of subjects are closed together, it is hard for the edge detection algorithm to draw out the hand contour properly. To address the second problem, researchers proposed the PRE ROI extraction method to extract the ROI area in complex background, but still requires subjects to keep their fingers open (Chai et al. 2016).

To address the two problems aforementioned and simplify the steps of ROI extraction, we proposed a deep learning ROI extraction method based on Blaze Palm (Bazarevsky and Zhang 2019), Google pre-trained hand tracking model. The model is mainly composed of a whole palm detector and a hand key point locator. The whole palm detector uses an oriented hand bounding box to locate the palm in the image, which avoids threshold choosing. The key point locator will locate hand key points in the cropped hand bounding box. The model uses 30,000 hand images with manually labeled key point data as training set, including real hand images photoed in different scenes and synthetic images generated by computers. The luminance conditions and finger positions in the training set are variable, so the model is robust in different environments and can address the problems mentioned above.

The detailed steps of REM is shown in the first block of Fig. 2a. We convert the color image into the grayscale image. And second, we apply BlazePalm to locate two key points in the hand, one index finger root node named A1, and the other is the pinky finger root node named A2. We connect A1 and A2, and calculate the length L of line A1A2 and the angle θ between the line A1A2 and the horizontal line. We use a square box to represent the ROI area, with A1A2 as one side of the square. Third, as the palm positions in different images are different, the selected ROI needs to be aligned to facilitate the subsequent principal line feature extraction. We take A2 as the center of rotation, and θ as the rotation angle, then rotate the ROI area counterclockwise to horizontal.

To measure the extraction performance, REM calculates the sum of the Euclidean distance between the vertex coordinates of the extracted ROI area and the vertex coordinates of the corresponding ground truth ROI area. If the sum of the distances is less than the chosen threshold, we consider the extraction to be successful, if it is greater than the threshold, the extraction failed. The evaluation metric is accuracy, and the calculation method is shown in the following formula.

$$\text{acc} = \frac{1}{N}\sum_{i=1}^{N} I(\text{ED}(\text{ROI}_i^{gt}, \text{ROI}_i) - c) \tag{1}$$

Where N is the number of test images, ROI_i^{gt} is the i_{th} manually labeled ground truth ROI image, and ROI_i is the i_{th} ROI area obtained from the ROI extraction method. c is the distance threshold, and $\text{ED}(\cdot,\cdot)$ is the Euclidean distance function which calculates the distance between two ROI's vertexes.

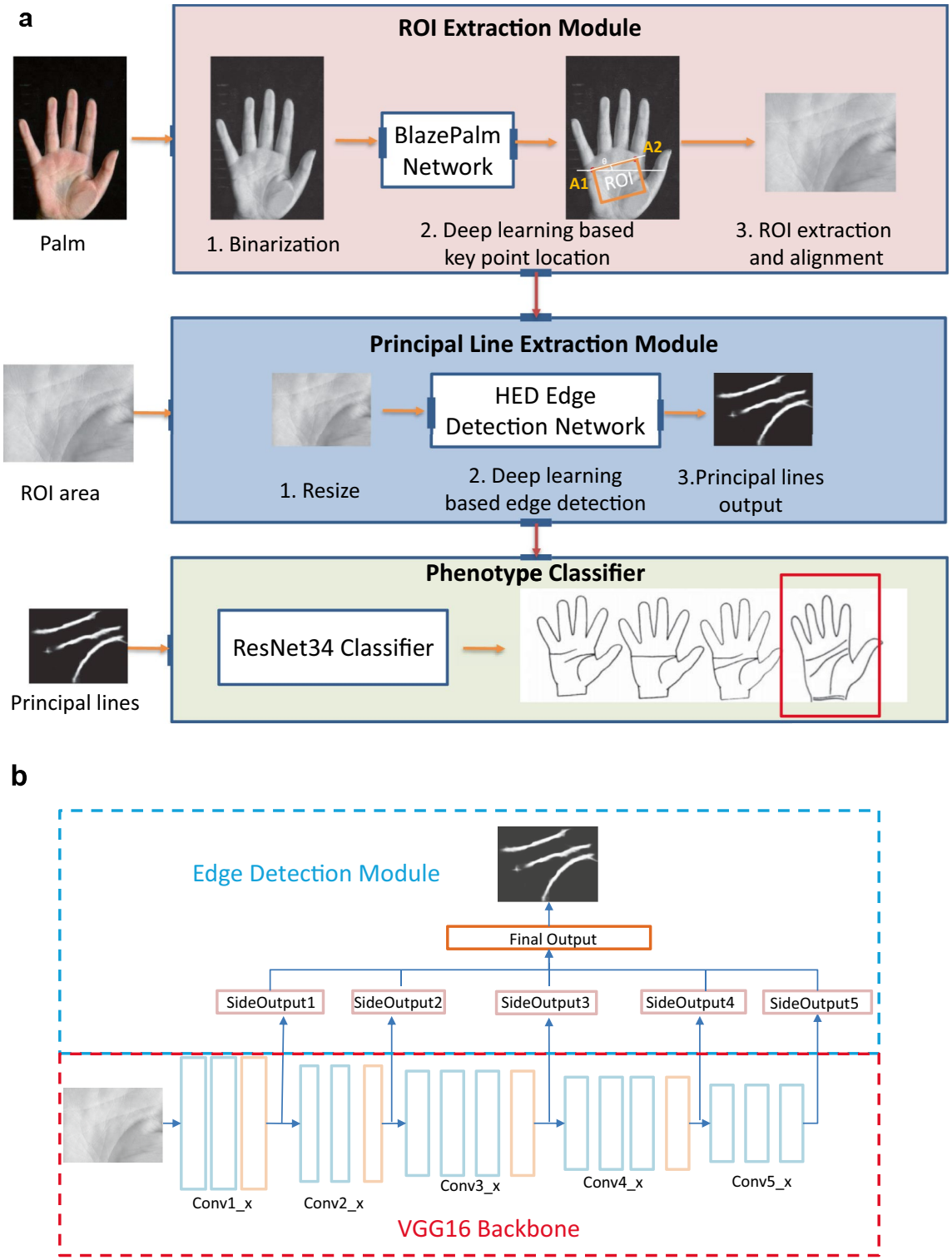

Fig. 2 Architecture of our model. **a** Our proposed model architecture, including REM, PLEM and PC. **b** Details about PLEM, i.e. the HED model, including VGG16 Backbone for feature extraction and Edge Detection Module for edge line extraction, and input is gray-scale ROI area and output is the binary principal line image

I is the indicator function, $I(x) = 1 \text{ if } x > 0,$ $I(x) = 0 \text{ if } x \leq 0.$

PLEM

After ROI extraction, we obtained the ROI area, including the three deepest and longest palmprint principal lines, as well as the small crest lines, folds, and other features. To reduce computation resource cost, the first step of our PLEM is to resize the input ROI areas into $200 * 150$ gray images, and the output of the PLEM is binary images of principal lines.

Traditional edge detection operator is mainly designed based on the gray-scale transformation. But for the contact-based palmprint images, there exist wrinkles caused by extrusion between palms and palm collection device. Such wrinkles will interfere with the principal line extraction. Deep learning edge detection algorithm not only uses the gray-scale transformation information but also other potential features, such as the direction of the line, the length of the line. And we build our PLEM based on the holistically nested edge detection network (HED) (Xie and Tu 2015).

Deep convolutional neural network is composed of many layers, and different layers can learn different hierarchical features. Shallow layers can extract the basic physical features, and with the depth of layers increasing, high-level feature can be extracted, such as principal lines. To fully utilize those different hierarchical features, researchers have proposed many different hierarchical learning and multi-scale learning methods, including DeepContour (Shen et al. 2015), CaseNet (Yu et al. 2017), and HED (Xie and Tu 2015). As HED model and its variants show promising results in many fields, we choose HED model as our palmprint principal line extraction model.

The architecture of Holistically-nested Edge Detection model is shown in Fig. 2b, which utilizes VGG16 network as backbone. The model is comprised of two parts, that is, the VGG16 backbone and the edge detection module. The VGG16 backbone includes five stages with different receptive fields, and the edge detection module will learn multi-scale features from the output of different VGG16 stages. The structure of five VGG16 stages is several convolutional layers followed by a max pooling layer with stride 2. Conv1: two convolutional layers with 64 kernels of size 3; Conv2: two convolutional layers with 128 kernels of size 3; Conv3: three convolutional layers with 256 kernels of size 3; Conv4 and Conv5: three convolutional layers with 512 kernels of size 3. Compared with original VGG16 network, HED has the following modifications:

1. The last three fully connected layers and the last pooling layer of VGG16 network are eliminated because we only need the multi-scale features of intermediate layers and do not need fully connected layers to do image classification tasks.
2. The edge detection module connects a side output layer to the last convolutional layer of each stage. So HED model can learn different scale features. And the output of five side output layers is concatenated as the input of the final output layer.
3. A new loss function is proposed, which considers the difference between all side output layers and the ground truth edge image. The integration of each side output layer prediction is more accurate than a single final output layer prediction.

In terms of evaluation metrics, the main purpose of the edge detection model in this paper is to extract the main structure of palmprint principal lines. The focus is to measure the main structural similarity between the extracted results and the original principal lines, regardless of whether a small number of pixels is classified right or wrong. Therefore, this paper uses SSIM (Hore and Ziou 2010) as the evaluation metric, instead of accuracy or F1 Score. SSIM measures the similarity of two images based on three characteristics: luminance, contrast, and structure. SSIM is defined as follows:

$$\text{SSIM}(x, y) = l(x, y) \cdot c(x, y) \cdot s(x, y) = \frac{(2\mu_x\mu_y + c_1)(2\sigma_{xy} + c_2)}{(\mu_x^2 + \mu_y^2 + c_1)(\sigma_x^2 + \sigma_y^2 + c_2)} \tag{2}$$

$l(x, y)$ measures the luminance similarity between image x and image y, μ_x and μ_y is the mean value of image x and y, c_1 and c_2 are two constant to avoid zero division. $c(x, y)$ measures the contrast similarity between the image, σ_x and σ_y are the standard deviation of the pixel value. $s(x, y)$ calculates the structure, and μ_{xy} is the covariance of two images. And SSIM is the integration of these three aspects.

Phenotype Classifier

To divide the palmprint principal lines into different palmprint phenotypes, we need to build our phenotype classifier. As neural network has shown promising results in image classification (He et al. 2016), we choose different neural networks as our phenotype classifier, including ResNet18, ResNet34, a three-layer fully-connected network, and a three-layer convolutional network. We compare their results and choose the one with the highest performance.

ResNet is proposed to overcome the Degradation Problem. ResNet designs a special Residual Block which can alleviate Degradation Problem and make neural network have higher learning ability. ResNet has many variants according to the depth of different models, such as ResNet18, ResNet34 and ResNet152. As the extracted palmprint images are very simple and only contain several principal lines and black background, a very deep neural network may lead to the

problem of overfitting. So we choose ResNet34 as the classification model, to balance the trade-off between the learning ability and the risk of overfitting. Besides, we utilize the idea of transfer learning. We initialize the ResNet classifier with parameters pre-trained on the ImageNet dataset.

Results

ROI Extraction

In this section, we compare our deep learning ROI extraction method with the Kekre valley point based ROI extraction method (Kekre et al. 2012), and Chai's PRE method (Chai et al. 2016). Because the database is relatively new, there is no recognized ground truth ROI area yet. Therefore, in this section, 500 palmprint images are randomly selected from the self-built palmprint database to evaluate the performance of different ROI extraction methods. And these 500 images of the ROI area are manually labeled as the ground truth image of the measurement standard by the experts in the palmprint research field.

Our deep learning method gets 21 failed cases without ROI area output, which means the method can not find key points in the hand. In the 479 cases of extracted ROI area, three cases are abandoned due to the distance between extracted ROI area and ground truth ROI area larger than the threshold. Our method has 476 successful cases with a extraction successful rate of 95.2%, the highest among all methods. Chai's method is 6% lower than our method, but still much better than the Kekre finger valley point extraction method. This result indicates our method can extract the great majority of ROI area in the dataset, while Chai's method and Kekre's method perform poorly because they cannot handle the situation when the fingers of subjects are closed together. The results of our experiments are summarized in Fig. 3. Then we utilize our deep learning method to extract the ROI area of all 5251 palm images in the dataset. Each image contains two hands, so the dataset includes 10,502 images of ROI area, and our deep learning method output 9941 images of ROI area, and 561 failed cases.

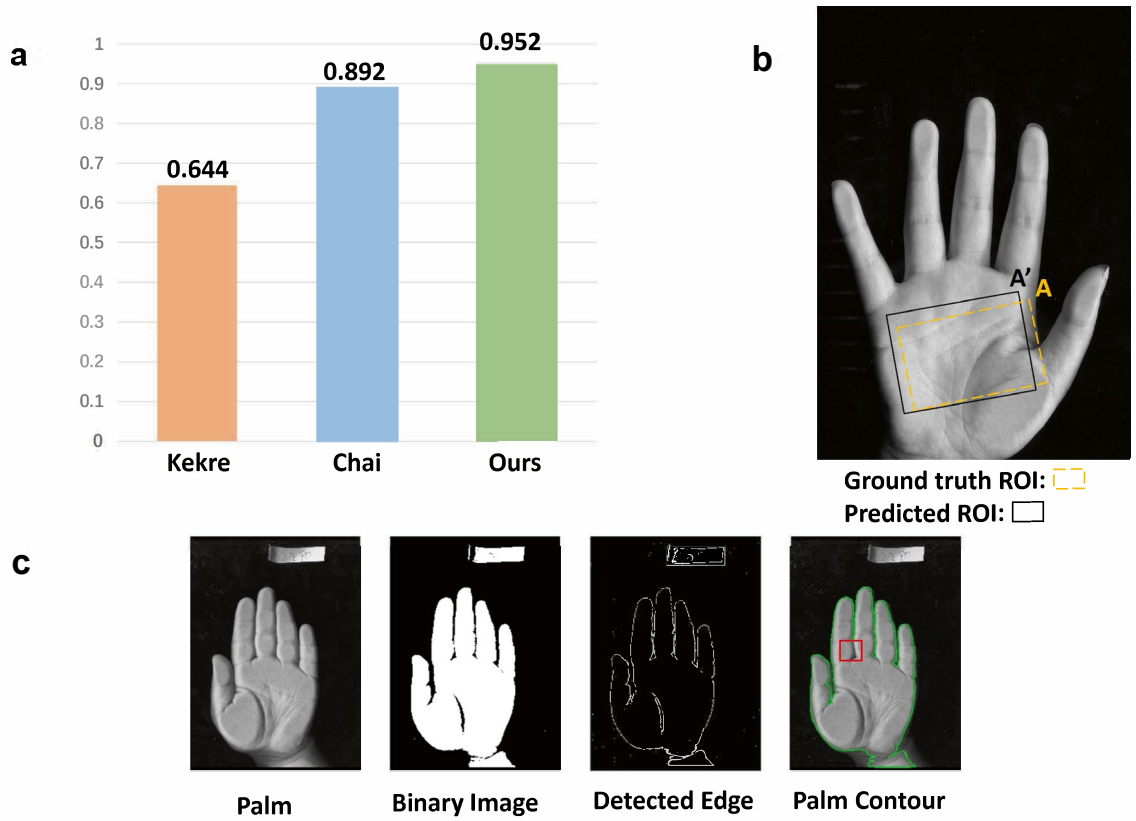

Fig. 3 Procedure and results of ROI extraction. **a** The result of ROI extraction success rate using Kekre's method, Chai's method, and our own method. **b** An example of ROI extraction, including the ground truth ROI area and predicted ROI area. We calculate the distance between two ROI's vertexes, for example, the distance between A and A'. If AA' is smaller than the distance threshold c, we regard it as a successful extraction case. **c** An example of failed cases, the extracted contour is in green, while the palm contour in the red box is not detected properly, leading to the failure of valley point location and ROI extraction

Principal Line Extraction

In this section, the holistically nested edge detection model and four traditional edge detection operators (Ali et al. 2016) are used to extract principal lines. To evaluate their performance, we calculate the structural similarity between results and ground truth images. We manually label 480 principal line images as ground truth, apply 400 images to train the HED model, and evaluate the performance of different methods on the surplus 80 images. In addition, to improve the robustness of the deep learning model, we enhance the dataset by flipping the training images horizontally, vertically, both horizontally and vertically. So 1600 images are used for HED training. Here, HED uses default parameters as the author suggested.

We did the principal line extraction experiment using the Laplacian operator, Sobel operator, Scharr operator, Canny operator and our HED model. Results show our HED model has the highest SSIM value compared with traditional edge detection operators. To further discuss the difference between these methods, we compare the extracted principal lines. We can find as the vein texture on the palm is very complicated, traditional edge detection operators cannot distinguish the small wrinkle and the principal lines. While our HED network can utilize discriminative features to extract the principal lines clearly, and it has strong anti-interference ability. To explain the training process of HED model, we visualize the output of the HED intermediate layers. The results of principal line extractions are shown in Fig. 4.

Phenotype Classification

In this section, we utilize the aforementioned neural networks to classify palmprint phenotype. We utilize the ROI and extracted edges as the input for the classification model and compare their results. After ROI extraction we get 9941

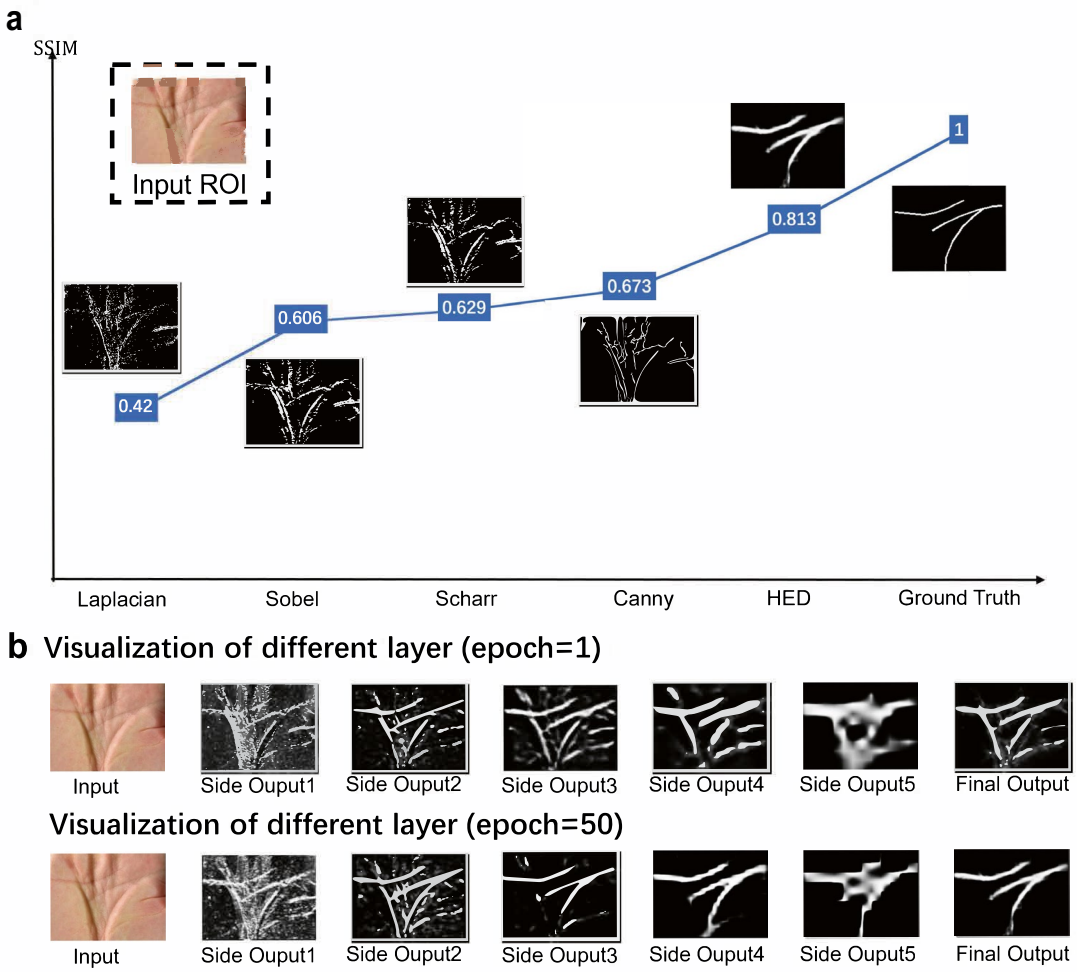

Fig. 4 Results of phenotype extraction. **a** Principal line extraction results comparison using different edge detection operators and HED model. **b** Visualization of intermediate layers of HED model in the first training epoch 1 and last epoch 50

images of ROI areas, and the phenotype distribution of these images is shown in Table 1. We divide the data according to the ratio of training set: validation set: test set = 8:1:1. It is noted that there is a serious data imbalance problem in the sample, and the normal type accounts for more than 90%. Therefore, we apply data enhancement method in the Triple radial base crease palmprints, Simian palmprints, and Sydney type, and we rotated these images horizontally, vertically, both horizontally and vertically. The validation set and test set are not enhanced. The final phenotype data distribution is shown in Table 1.

The evaluation metric is accuracy, learning rate is 0.001, batch size is 64, Adam optimizer is exploited with the default setting, and training epoch is 50. An RTX2080ti is used for network training. Table 2 shows the classification accuracy on testing set using different classification networks, and the best results are highlighted in bold.

For ROI images and edge images extracted by the HED network, Sobel Operator, and Laplacian Operator, using ResNet34 achieves the highest classification accuracy among these four networks, which reflects the strong feature extraction ability of ResNet34. And in these four networks, we can find using edge images extracted by HED outperforms directly using ROI images as inputs, which shows the advantage of our proposed architecture.

To further discuss the training process of ResNet34, we draw the classification accuracy curve of training set and validation set in Fig. 5. The ResNet34 model can achieve nearly 100% classification accuracy in training set using all kinds of inputs, while in the validation set using ROI images and edge images extracted by HED outperform other inputs. This result indicates traditional edge extraction operator may lose some useful information for classification, but our HED model keeps it. Table 3 shows the classification accuracy of different palmprint phenotypes using ResNet34. From which we can find using edges extracted by HED improves model performance in normal type, Simian type, and Sydney type compared with using ROI images, and the total accuracy increases 1.5%. We are also curious about the misclassified images, and Fig. 6 shows two typical misclassified Sydeny type images. Due to the complex distribution of principal lines, using ROI area or extracted lines images all fail to classify these two images into the right type.

Table 2 Accuracy on test set using different neural networks

Inputs	Three layers MLP	Three layers Conv	ResNet18	ResNet34
Sobel Edge	0.895	**0.889**	0.915	0.928
Laplacian Edge	0.881	0.889	0.921	0.923
Canny Edge	0.874	0.870	0.898	0.894
Scharr Edge	0.878	0.880	0.923	0.906
ROI	0.895	0.870	0.937	0.942
HED Edge	**0.923**	0.888	**0.943**	**0.957**

Bold indicates best performance

Discussion

Recent researches have shown many promising applications using palmprint feature. In the biometric field, researchers started to use geometry features, principal-line features, and wrinkle features to verify a person's identity (Shu and Zhang 1998). In the forensic crime investigation field, palmprint images in the criminal scene were collected to help detect the identification of masked terrorists (Chan et al. 2017). In the medical field, Cascos researched 150 patients with congenital heart disease and analyzed their palmprint pattern (Cascos 1965). Such applications require higher demands for palmprint feature extraction and phenotype classification.

To the best of our knowledge, this study builds the first deep learning architecture for palmprint phenotype feature extraction and classification, which includes ROI extraction, principal lines extraction and phenotype classification. This study builds a large palmprint phenotype dataset with 9941

Table 1 Distribution of training set, validation set and test set (without/with data enhancement)

Without enhancement	Normal	Simian	Triple radial base crease	Sydney	Total
Training	7168	238	521	25	7952
Validation	900	28	61	6	995
Test	890	37	61	6	994
Total	8958	303	643	37	9941
With enhancement	Normal	Simian	Triple radial base crease	Sydney	Total
Training (Enhanced)	7168	952	2084	100	10,304
Validation	900	28	61	6	995
Test	890	37	61	6	994
Total	8958	1017	2206	112	12,293

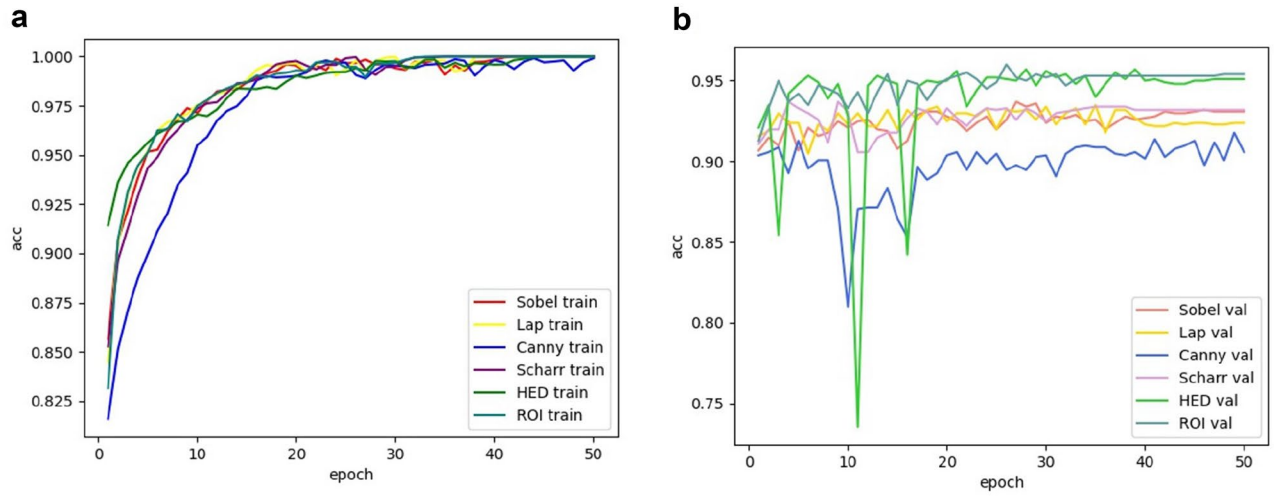

Fig. 5 Phenotype classification accuracy using ResNet34 **a** in the training set and **b** in the validation set

Table 3 Accuracy on test set using ResNet34

Inputs	Normal	Simian	Triple radial base crease	Sydney	Total
Sobel Edge	0.972	0.454	0.656	0	0.928
Laplacian Edge	0.967	0.432	0.639	0	0.923
Canny Edge	0.965	0.189	0.377	0	0.894
Scharr Edge	0.976	0.432	0.246	0.167	0.906
ROI	0.973	0.622	0.770	0	0.942
HED Edge	**0.983**	**0.703**	**0.770**	**0.500**	**0.957**

Bold indicates best performance

unique palms, and compares the performance of our method and traditional methods in the dataset. The result shows the effectiveness and reliability of our model.

To extract ROI areas, we need to find proper key points to build the coordinate system. Kekre calculates the distance between points in the hand contour and the centroid, and the points with the smallest distance are valley points. Chai regards the hand as a small convex hull, and the valley points are the farthest in convex defects to the convex hull. Both methods need precise hand contour tracking, while it will be difficult to get hand contour when the subject fingers are closed or the luminance condition is complex. Our REM uses deep neural network BlazePalm to locate key points directly. And BlazePalm uses a large number of hand images in different postures and different environments for pre-training, and it is robust to irrelevant interference. By further discussing the failed cases, we can find traditional methods perform poorly in three situations; first, the fingers are closed together; second, the ROI area hanging in the air; third, the subjects wear a ring. Figure 3c shows one typical failed case of the Kekre ROI extraction method. Due to the subject's fingers being closed, the detected palm contour is not complete, and the valley point between the index finger and middle finger is not included in the palm contour, leading to the failure of the valley point location.

In the principal line extraction task, we use four edge detection operators and HED edge detection network to extract the lines. Traditional edge detection operators rely on the grayscale value change to find the edge, but the edges on the palmprint include principal lines, small crest lines, and folds. So the result produced by edge detection operators contains much noise information. In Fig. 4c, we visualize the output from different layers of our HED edge

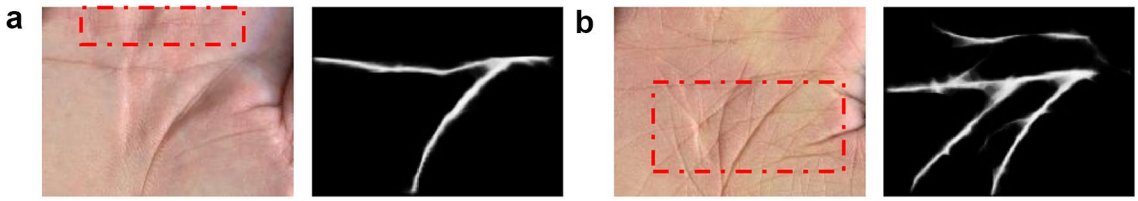

Fig. 6 Two typical misclassified cases **a** the principal line in red box is too shallow, so it cannot be captured by the PLEM, which leads to the wrong classification, and **b** the lines in the red box have similar directions and similar depth, so both lines are extracted, which makes it difficult for the classifier to recognize

detection model in different periods. We choose the output of epoch1, the starting epoch, and the output of epoch50, the last epoch in which the loss of HED model is nearly convergent. The output from shallow layers is similar to the edge detection operator output, containing principal lines, wrinkles, and many other useless features. With the layers becoming deeper, HED model will filter useless features and keep the principal lines feature. Such a process makes HED model achieve a higher SSIM value (0.813) compare with traditional edge detection operators.

For phenotype classifying, we choose a famous deep learning network ResNet34, and compare the results by different inputs. We use the edge extracted by the edge detection operator, the original ROI area, and the edge extracted by HED model. We can find that using edges extracted by HED has the highest classification accuracy 95.7% and using the original ROI area has the second highest accuracy. But using edges extracted by traditional edge detection operators has relatively lower accuracy. The reason accounting for this result may be that traditional edge detection operator lose some useful information for phenotype classifying. And in the contrast, our HED edge detection model keeps useful information and improves final performance.

This study also has some limitations. First, we only discuss the feature extraction and phenotype classifying of palmprint, and we can apply our model in other dermatoglyphics or extend our model to other palmprint dataset. Second, there still exists a large space for further analysis of the relationship between palmprint phenotype and gene type. Last, the performance of the model in rare classes needs improvement due to the serious data imbalance problem. All the work will be considered in the future study.

Conclusion

In this paper, a palmprint phenotype classification architecture is proposed, including REM, PLEM, and PC. In the REM, we utilize a pre-trained hand key point location model to improve the ROI extraction performance in complicated situations. For the PLEM, it's the first palmprint principal line extraction model using deep neural network. And the comparison between our model and traditional edge detection operators shows the strong feature learning ability of our model, with 0.813 SSIM value. And we use the extracted principal lines to do palmprint phenotype classification task and achieve an accuracy of 95.7%. Also, we build a new manually labeled dataset for ROI extraction, principal line extraction, and phenotype classification. For future development, we hope to apply the extracted principal line feature for other tasks such as palmprint recognition and further investigate the use of deep learning methods for other dermatoglyphics feature extraction and utilization.

Author's Contributions GZ and SW conceived the project and provided main resources. YF constructed the principle network frame. JL conducted data collection, investigation and curation. JL, SS and HZ labeled the classification of palmprint phenotype feature of CAS_palm set. YF and JL wrote the original draft.

Funding We would like to thank the participants of the CAS_palm set who consented to participate in research. This project was funded by the Shanghai Municipal Science and Technology Major Project 2017SHZDZX01 (S.W.), National Natural Science Foundation of China Grant 61831015 (G.Z.) and China Postdoctoral Science Foundation Grant 2019M651351 (J.L.).

Data Availability The raw images on individuals are not readily available. The code for ROI extraction and Network construction will be released after the article is accepted.

Declarations

Conflicts of Interest All of authors declare no competing interests.

Ethics Approval All participants provided written informed consent, and all study protocols were approved by the institutional review boards of the pertinent research institutions. This CAS_palm set consists of data from the project which was approved by the Ethics Committee of Human Genetic Resources at the Shanghai Institute of Life Sciences, Chinese Academy of Sciences (ER-SIBS-261410-A1801).

Consent to Participate Written informed consent was obtained from each of the volunteers.

Consent to Publication All the participants approved to publish the paper.

References

Ali MM, Yannawar P, Gaikwad A (2016) Study of edge detection methods based on palmprint lines. In: 2016 International Conference on Electrical, Electronics, and Optimization Techniques (ICEEOT), IEEE, pp 1344–1350. https://doi.org/10.1109/ICEEOT.2016.7754902

Badrinath G, Gupta P (2012) Palmprint based recognition system using phase-difference information. Fut Gen Comput Syst 28(1):287–305. https://doi.org/10.1016/j.future.2010.11.029

Bazarevsky V, Zhang F (2019) On-device, real-time hand tracking with mediapipe. Google AI Blog. https://doi.org/10.48550/arXiv.2006.10214

Bruno A, Carminetti P, Gentile V, La Cascia M, Mancino E (2014) Palmprint principal lines extraction. In: 2014 IEEE Workshop on Biometric Measurements and Systems for Security and Medical Applications (BIOMS) Proceedings, IEEE, pp 50–56, https://doi.org/10.1109/BIOMS.2014.6951535

Cascos AS (1965) Palm-print pattern in congenital heart disease. Br Heart J 27(4):599

Chai T, Wang S, Sun D (2016) A palmprint roi extraction method for mobile devices in complex environment. In: 2016 IEEE 13th International Conference on Signal Processing (ICSP), IEEE, pp 1342–1346. https://doi.org/10.1109/ICSP.2016.7878045

Chan FKS, Li X, Kong AWK (2017) A study of distinctiveness of skin texture for forensic applications through comparison with blood vessels. IEEE Trans Inform Foren Secur 12(8):1900–1915. https://doi.org/10.1109/TIFS.2017.2692684

He K, Zhang X, Ren S, Sun J (2016) Deep residual learning for image recognition. In: Proceedings of the IEEE conference on computer vision and pattern recognition, pp 770–778. https://doi.org/10.1109/CVPR.2016.90

Hore A, Ziou D (2010) Image quality metrics: Psnr vs. ssim. In: 2010 20th international conference on pattern recognition, IEEE, pp 2366–2369. https://doi.org/10.1109/ICPR.2010.579

Huang DS, Jia W, Zhang D (2008) Palmprint verification based on principal lines. Pattern Recogn 41(4):1316–1328. https://doi.org/10.1016/j.patcog.2007.08.016

Kekre H, Sarode T, Vig R (2012) An effectual method for extraction of roi of palmprints. In: 2012 International Conference on Communication, Information and Computing Technology (ICCICT), IEEE, pp 1–5. https://doi.org/10.1109/ICCICT.2012.6398207

Otsu N (1979) A threshold selection method from gray-level histograms. IEEE Trans Syst Man Cybern 9(1):62–66. https://doi.org/10.1109/TSMC.1979.4310076

Park JS, Shin DS, Jung W, Chung MS (2010) Improved analysis of palm creases. Anat Cell Biol 43(2):169–177. https://doi.org/10.5115/acb.2010.43.2.169

Prasad S, Chai T (2020) Palmprint for individual's personality behavior analysis. Comput J. https://doi.org/10.1093/comjnl/bxaa045

Shen W, Wang X, Wang Y, Bai X, Zhang Z (2015) Deepcontour: A deep convolutional feature learned by positive-sharing loss for contour detection. In: Proceedings of the IEEE conference on computer vision and pattern recognition, pp 3982–3991. https://doi.org/10.1109/CVPR.2015.7299024

Shu W, Zhang D (1998) Automated personal identification by palmprint. Opt Eng 37:2359–2362. https://doi.org/10.1016/j.patcog.2004.02.015

Wojtowicz H, Wajs W (2012) Intelligent information system for interpretation of dermatoglyphic patterns of down's syndrome in infants. In: Asian Conference on Intelligent Information and Database Systems, Springer, pp 284–293. https://doi.org/10.1007/978-3-642-28490-8_30

Xie S, Tu Z (2015) Holistically-nested edge detection. In: Proceedings of the IEEE international conference on computer vision, pp 1395–1403. https://doi.org/10.1016/0146-664X(82)90070-3

Yu Z, Feng C, Liu MY, Ramalingam S (2017) Casenet: Deep category-aware semantic edge detection. In: Proceedings of the IEEE conference on computer vision and pattern recognition, pp 5964–5973. https://doi.org/10.1109/CVPR.2017.191

Zhai G, Min X (2020) Perceptual image quality assessment: a survey. Sci China Inform Sci 63(11):1–52. https://doi.org/10.1007/s11432-019-2757-1

Zhai G, Zhang W, Yang X, Xu Y (2005) Image quality assessment metrics based on multi-scale edge presentation. In: IEEE Workshop on Signal Processing Systems Design and Implementation, 2005., IEEE, pp 331–336. https://doi.org/10.1109/SIPS.2005.1579888

Zhang L, Li L, Yang A, Shen Y, Yang M (2017) Towards contactless palmprint recognition: a novel device, a new benchmark, and a collaborative representation based identification approach. Pattern Recogn 69:199–212. https://doi.org/10.1016/j.patcog.2017.04.016